



# Assessment of structural materials containing notch-type defects: A comprehensive validation of the FAD-TCD methodology on metallic and non-metallic materials

Sergio Cicero

LADICIM, Departamento de Ciencia e Ingeniería del Terreno y de los Materiales, University of Cantabria, Avenida de los Castros, 44, 39005 Santander, Spain

## ARTICLE INFO

### Keywords:

Structural material  
Structural integrity  
Notch  
Failure assessment diagram  
Theory of critical distances  
Line method

## ABSTRACT

This paper provides a comprehensive description, and the subsequent validation, of a structural integrity assessment methodology of structural materials containing notch-type defects. The approach is based on the combination of Failure Assessment Diagrams (FAD) and the Theory of Critical Distances (TCD). The former provides the general assessment tool, which is exactly the same one as that used for crack-like defects, whereas the latter provides the notch effect correction required for the analysis of this type of defects. Finally, the proposed methodology is validated on a number of metallic and non-metallic structural materials, with 1,106 experimental results on different types of testing specimens, covering four structural steels, aluminium alloys 7075-T651 and 6060-T66, PVC, PMMA, PA6, fibre-reinforced PA6, 3D printed (Fused Filament Fabrication) ABS, PLA and graphene reinforced PLA, granite and limestone. The results show how the FAD-TCD methodology provides safe reasonably conservative assessments on the mentioned structural materials in the presence of notch-type defects.

## 1. Introduction

The structural integrity assessment of components containing cracks is a well-defined process in the most recognized structural integrity assessment procedures, such as BS7910 [1], API 579-1/ASME FFS-1 [2] or R6 [3]. When dealing with fracture/plastic collapse assessments (i.e., when fatigue, creep and other subcritical processes are not evaluated), the main assessment tool provided by such procedures is the Failure Assessment Diagram approach, which is based on the definition of three different concepts:

- $K_r$ : the fracture ratio of applied stress intensity factor ( $K_I$ ) to material fracture toughness ( $K_{mat}$ ). It defines the condition against fracture.

$$K_r = \frac{K_I}{K_{mat}} \quad (1)$$

Assessment procedures provide solutions of  $K_I$  for a wide number of practical situations. Regarding  $K_{mat}$ , it represents the material fracture resistance, which may fulfil linear-elastic conditions (e.g.,  $K_{IC}$ ) or may be elastic-plastic (e.g.,  $K_J$ ).

- $L_r$ : the ratio of applied load ( $P$ ) to limit load ( $P_L$ ), defining the condition against plastic collapse. It may be also defined as the ratio of the reference stress ( $\sigma_{ref}$ ) to the yield ( $\sigma_y$ ) or proof stress ( $\sigma_{0.2}$ ). Again, assessment procedures provide solutions of  $P_L$  (or  $\sigma_{ref}$ ) for a wide number of practical situations.

$$L_r = \frac{P}{P_L} = \frac{\sigma_{ref}}{\sigma_y} \quad (2)$$

- FAL: the Failure Assessment Line, defining the critical condition.

$$K_r = f(L_r) \quad (3)$$

Structural integrity assessment procedures provide different  $f(L_r)$  functions, which are actually plasticity corrections to the linear-elastic fracture assessment, and whose exact solution is:

$$f(L_r) = \sqrt{\frac{J_e}{J}} \quad (4)$$

$J$  being the applied J-integral and  $J_e$  being the elastic component of  $J$ . This plasticity correction allows the  $K_r$  ratio to be defined from a linear-elastic parameter ( $K_I$ ) and a non-necessarily linear-elastic material property ( $K_{mat}$ ). When  $K_{mat}$  deviates from linear-elastic conditions and,

E-mail address: [ciceros@unican.es](mailto:ciceros@unican.es).

<https://doi.org/10.1016/j.tafmec.2024.104612>

Received 16 July 2024; Received in revised form 8 August 2024; Accepted 8 August 2024

Available online 10 August 2024

0167-8442/© 2024 The Author(s). Published by Elsevier Ltd. This is an open access article under the CC BY-NC license (<http://creativecommons.org/licenses/by-nc/4.0/>).

Nomenclature			
a	crack length	W	specimen width
$A_p$	plastic area under the load–displacement curve in a fracture test	$\eta$	dimensionless constant
$b_0$	initial remaining ligament	$\sigma_f$	flow stress
B	specimen thickness	$\sigma_{ref}$	reference stress
$e_{max}$	strain under maximum load	$\sigma_y$	yield stress
E	elastic modulus	$\sigma_u$	ultimate tensile strength
$f(L_r)$	function of $L_r$ defining the FAL	$\sigma_{0.2}$	0.2 % proof strength
J	J integral	ABS	Acrylonitrile butadiene styrene
$J_c$	material fracture toughness measured by J integral	CF	Conservatism Factor
$J_e$	elastic component of J	CT	Compact tension specimen
$K_J$	crack driving force (J) in stress intensity factor units	DBTR	Ductile-to-brittle transition region
$K_{mat}$	material fracture toughness	FAD	Failure Assessment Diagram
$K_{mat,avg}$	average material fracture toughness	FAL	Failure Assessment Line
$K_{mat,0.05}$	material fracture toughness associated to a 5 % tolerance bound	FFF	Fused Filament Fabrication
$K_{mat}^N$	material apparent fracture toughness	LM	Line Method
$K_r$	fracture ratio of applied $K_I$ to fracture resistance	MC	Master Curve
$K_I$	stress intensity factor	PA6	Polyamide 6
$L_r$	ratio of applied load to limit load (or reference stress to yield stress)	PLA	Polylactic acid
P	applied load	PLA-Gr	Graphene reinforced PLA
$P_L$	limit load	PM	Point Method
$P_L^N$	notch limit load	PMMA	Polymethyl methacrylate
N	strain hardening exponent	PVC	Polyvinyl chloride
$T_0$	Reference temperature defining the Master Curve	SENB	Single edge notched bending specimen
		SGF	Short glass fibre
		SGFR <sub>x</sub> -PA6	Short glass fibre reinforced polyamide 6 (x wt.% content of SGF)
		TCD	Theory of Critical Distances

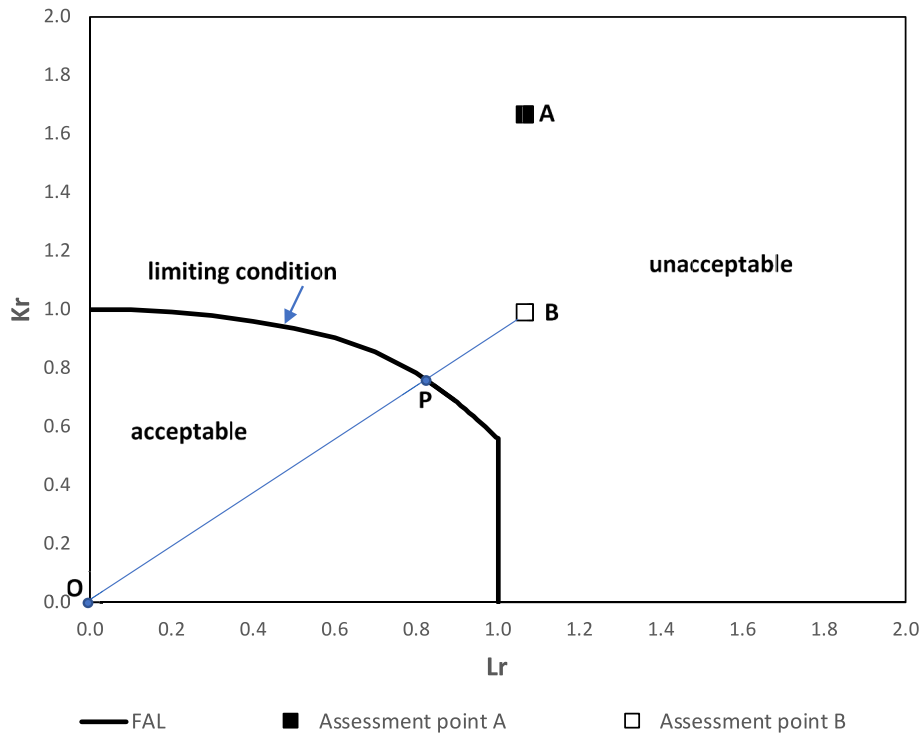


Fig. 1. Schematic of a FAD assessment, with the assessment points (A and B) representing unacceptable situations of the components being analysed.

thus, from the direct comparison between  $K_I$  and  $K_{IC}$ ,  $f(L_r)$  actually converts the fracture assessment into a comparison between the applied J and the material critical J ( $J_c$ ).

In reality, structural integrity assessment procedures (e.g., [1–3])

offer approximate solutions to (4), which are simply defined through the tensile properties of the material. These solutions are usually provided hierarchically, with distinct levels of approximation to equation (4) depending on the level of detail in the definition of the tensile curve.

Thus, the better the knowledge about the tensile curve, the better the definition of the failure evaluation line and the higher the accuracy of the analysis. As an example, BS7910 [1] defines three analysis options, with Option 1 defining the FAD from the material yield stress (or proof stress), ultimate tensile strength, elastic modulus and yielding behaviour (continuous/discontinuous yielding), Option 2 defining the FAD through the complete uniaxial tensile true stress–strain curve, and Option 3 defining the FAD through equation (4) (exact solution). Option 1 and 2 provide, therefore, simplified conservative approximations to Option 3.

Then, in a  $K_r$ - $L_r$  graph,  $K_r$  and  $L_r$ , as defined by equations (1) and (2), determine the coordinates of the point representing the component being assessed. The situation of such a point regarding the FAL establishes whether or not it is working under safe or unsafe conditions: if the point is located within the area defined by the FAL and the coordinate axes, it operates in acceptable (safe) conditions; if the point is located above the FAL, the component condition is unacceptable (unsafe); if the point is located exactly on the FAL, it is exactly at limiting (failure) conditions. Fig. 1 provides a schematic of the FAD approach, with points A and B representing two unacceptable conditions.

The above-described analysis process refers to fracture initiation analyses. Here, it is important to note that assessment procedures generally gather an analogous approach for ductile tearing analyses, where the component is represented by a locus of assessment points rather than by a single assessment point. For this and other additional details on FAD methodology, such as the specific equations of the different  $f(L_r)$  solutions, the reader is referred to the specific assessment procedures (e.g., [1–3]) and to scientific literature (e.g., [4–8]).

Moreover, the application of structural integrity assessment procedures and, consequently, the FAD approach described above on which fracture analyses are based, is limited to metallic materials and structures and to the assessment of crack-like defects. Thus, the structural integrity (FAD) assessment of non-metallic components and/or notch-type defects cannot, theoretically, be accomplished by using such procedures.

In this sense, the existence of structural components made of non-metallic materials is nowadays an evident reality (e.g., [9–11]), and the application of FADs to this kind of materials when containing crack-like defects has been addressed in some works (e.g., [12,13]), providing justification and validation to such a practice. Details on this issue will be provided below.

Concerning the assessment of structural components containing notches, this type of defects is very common in practice. In fact, there are recurrent situations, such as mechanical damage, corrosion defects, drilled holes, pores or fabrication defects (among others) where the existing defects threatening the integrity of the corresponding structural component are not infinitely sharp (i.e., crack-like) defects. On the contrary, they present a finite radius on their tip that relaxes the stress field and may even cause a change in the fracture micromechanisms [14–16]. These defects are generally referred to as notches or notch-type defects. When assessing components containing notches, it may be overly conservative to assume that they behave like cracks and, subsequently, to apply fracture mechanics approaches, including FADs. The scientific and technical literature shows (e.g., [14–21]) how notched materials develop an apparent fracture toughness ( $K_{mat}^N$ ) which is greater than the fracture toughness ( $K_{mat}$ ) developed when containing cracks, with direct consequences on the resulting load-bearing capacity and on the structural integrity. Hence, the assessment of the fracture behavior of notched materials should be made using specific criteria (e.g., [17–22]), among which the Theory of Critical Distances (TCD) stands out and has been widely validated [18]. Moreover, as it will be shown below, the TCD is capable of generating structural integrity assessment criteria for notched components [23] by combining its fracture criteria with the FAD approach. Again in Fig. 1, regarding the two unacceptable conditions represented by A and B, actually, and as it will be explained in detail below, these two points represent the average assessment

points at failure of all the experimental tests analyzed in this work, without and with the notch correction proposed by the author, respectively. It may be easily observed that the proposed notch correction generates a vertical displacement of the assessment point, while the  $L_r$  coordinate remains unchanged.

Concerning fracture assessments, the TCD is actually a group of different methodologies (e.g., Point Method, Line Method, Area Method and Volume Method) [18] that make use of a material length parameter (the critical distance,  $L$ ), together with the material fracture toughness, to determine the corresponding critical conditions.  $L$  is defined by:

$$L = \frac{1}{\pi} \left( \frac{K_{mat}}{\sigma_0} \right)^2 \quad (5)$$

$\sigma_0$  being the material inherent strength. As an example, the Point Method (PM) affirms that fracture takes place when the stress at a distance of  $L/2$  from the crack tip equals the material inherent strength:

$$\sigma \left( \frac{L}{2} \right) = \sigma_0 \quad (6)$$

Alternatively, the Line Method (LM) assumes that fracture takes place when the average stress along a distance equal to  $2L$  (measured from the notch tip), reaches  $\sigma_0$ :

$$\frac{1}{2L} \int_0^{2L} \sigma(r) dr = \sigma_0 \quad (7)$$

The Area Method and the Volume Method have analogous definitions [18]. The TCD can also be applied to fatigue analyses [18] and environmental assisted cracking analyses [24], in both cases through an adequate reformulation of equations (5) to (7).

With all this, Section 2 in this paper describes the FAD-TCD methodology used to analyse notched structural components, justifying its use not only in metals but also in non-metals; Section 3 describes the materials analyzed in this work (metals and a number of non-metals), gathering their relevant mechanical properties; Section 4 systematically presents the results obtained when applying the FAD-TCD methodology to the materials described in the previous section; Finally, Section 5 gathers the main conclusions.

## 2. FAD-TCD methodology

The methodology applied in this work to analyze notched structural materials is based on the combination of the FAD approach with the Theory of Critical Distances [23]. As shown above, FAD analyses require defining three different issues ( $K_r$ ,  $L_r$  and  $f(L_r)$ ), whose definition has to be addressed when dealing with notch-type defects:

- $K_r$ : in [14–21] it is revealed how the existence of a finite radius on the defect tip increases the fracture resistance of the material. The fracture resistance of a given material in notched conditions, usually referred to as the apparent fracture toughness ( $K_{mat}^N$ ) is, thus, generally higher than that developed in cracked conditions (fracture toughness,  $K_{mat}$ ).  $K_{mat}^N$  is determined by using similar fracture testing specimens to those used to define  $K_{mat}$  (e.g., CT or SENB specimens), with the difference that the defect introduced in the specimen and causing the fracture process is a notch, instead of a fatigue pre-crack (or any other type of crack-like defect). Moreover, once the test is performed and in order to quantify  $K_{mat}^N$ , one must follow the formulation provided by the corresponding standard (e.g., [25–27]) for crack-like defects (e.g.,  $K_I$  formulation,  $J$  formulation, etc). Therefore, when defining  $K_r$  for notch-type defects,  $K_{mat}$  must be substituted by  $K_{mat}^N$ , accounting for the actual fracture resistance developed by the material, and  $K_I$  remains as in crack-like defects, given that the  $K_{mat}^N$  itself is obtained through the ordinary fracture mechanics formulations, with  $K_I$  (or  $J$ ) as the crack-driving force:

$$K_r = \frac{K_I}{K_{mat}^N} \quad (8)$$

- $L_r$ : this parameter of the FAD approach evaluates the situation of the component against plastic collapse, which occurs through the yielding of the remanent section. In an ideal perfectly plastic material (with no hardening) which is capable of developing large plastic strains, it can be defined by the material yield stress and the defect dimensions, with no influence of the notch, given that (at failure) the defect does not act as a stress riser, it just reduces the resistant section. Thus, the plastic collapse, and the corresponding limit load, does not depend on the notch tip and it is (ideally) the same for notches and cracks (which are essentially infinitely sharp notches with negligible notch radius). In practice, materials do not have perfectly plastic behavior, and there may be certain notch effect on the limit load, but [28] demonstrates the low influence of the notch radius on  $P_L$ . Consequently,  $L_r$ , when analyzing notches through FADs, keeps the same definition as that used for crack-like defects (equation (2)), using the same  $P_L$  solutions (or  $\sigma_{ref}$  solutions) as those provided for cracks in structural integrity assessment procedures. This practice is a slightly conservative assumption that simplifies considerably the assessment process. This being said, if a specific solution of the limit load was available for the component and notch geometry being evaluated ( $P_L^N$ ), this could be directly considered in equation (2), instead of  $P_L$ .
- $f(L_r)$ : the exact solution of  $f(L_r)$  (equation (4), Option 3 in BS7910 [1]) may be applied in notched conditions. Horn et al demonstrated in [29] that there is a very weak dependence of equation (4) on the notch radius. However, engineering practice generally makes use of simplified solutions of  $f(L_r)$ , and particularly makes use of BS7910 Option 1, which is defined from basic tensile properties as follows: equations (9) to (14) for materials exhibiting continuous yielding; equations (15) to (21) for materials with discontinuous yielding (i.e., with yield plateau).

$$K_r = f(L_r) = \left[1 + \frac{1}{2}(L_r)^2\right]^{-1/2} \cdot \left[0.3 + 0.7 \cdot e^{-\mu \cdot (L_r)^6}\right] \quad L_r \leq 1 \quad (9)$$

$$K_r = f(L_r) = f(1) \cdot L_r^{\frac{N-1}{2N}} \quad 1 < L_r \leq L_{r,max} \quad (10)$$

$$K_r = f(L_r) = 0 \quad L_r = L_{r,max} \quad (11)$$

$$\mu = \min\left[0.001 \cdot \frac{E}{\sigma_{0.2}}; 0.6\right] \quad (12)$$

$$N = 0.3 \cdot \left(1 - \frac{\sigma_{0.2}}{\sigma_u}\right) \quad (13)$$

$$L_{r,max} = \frac{\sigma_{0.2} + \sigma_u}{2 \cdot \sigma_{0.2}} \quad (14)$$

$$K_r = f(L_r) = \left(1 + \frac{1}{2}(L_r)^2\right)^{-1/2} \quad L_r < 1 \quad (15)$$

$$K_r = f(L_r) = \left(\lambda + \frac{1}{2\lambda}\right)^{-1/2} \quad L_r = 1 \quad (16)$$

$$K_r = f(L_r) = f(1) \cdot L_r^{\frac{N-1}{2N}} \quad 1 < L_r < L_{r,max} \quad (17)$$

$$K_r = f(L_r) = 0 \quad L_r \geq L_{r,max} \quad (18)$$

$$L_{r,max} = \frac{\sigma_y + \sigma_u}{2 \cdot \sigma_y} \quad (19)$$

$$\lambda = \left(1 + \frac{E \cdot \Delta \varepsilon}{\sigma_y}\right) \quad (20)$$

$$\Delta \varepsilon = 0.0375(1 - 0.001 \cdot \sigma_y) \quad (21)$$

This BS7910 Option 1 FAD is the simplest analysis option of BS 7910. However, the standard specifically states that their application is limited to metallic materials. Thus, the structural integrity assessment of non-metallic components should not, theoretically, be performed using this option. The main reason behind this scope limitation is that  $\mu$  (equation (12)) and  $N$  (equation (13)) parameters follow expressions that have been calibrated and validated for metals [30–33], but not for non-metals. This is the main reason why structural integrity procedures such as FITNET FFS Procedure and BS7910 do not cover the fracture assessment of non-metallic materials. However, [12] demonstrates how equations (12) and (13) are also safe solutions for a wide variety of non-metallic materials with continuous yielding. Concerning discontinuous yielding materials, as they are basically metals, there is no need to validate the corresponding equations defining Option 1 FAD.

With all this, the FAD-TCD approach to assess the structural integrity of notched components is performed as in cracked components, with the only difference being found in the material fracture resistance that must be used to define  $K_r$ :  $K_{mat}^N$  instead of  $K_{mat}$ . The  $FAL$ ,  $K_I$  solutions and  $P_L$  solutions remain the same as in cracked assessments, so the expressions provided for all of them in structural integrity assessment procedures (e.g., [1–3]) may be directly used in the assessment of notches. When compared to the assessment of notches as if they were cracks (obviating the notch effect), the FAD-TCD methodology generates a vertical displacement of the assessment point, as it will be shown below in Section 4.

Finally, in order to solve the last question of the analysis,  $K_{mat}^N$  must be defined. In this sense, there is always the possibility of testing fracture mechanics specimens (e.g., CT, SENB) containing a notch with the same radius as that existing in the component being evaluated. However, there is also the possibility of applying the TCD, and particularly the LM, to determine  $K_{mat}^N$ . Assuming that  $L$  is known for the material of which the structural component is made, and combining the LM criterion (equation (7)) with the Creager-Paris stress distribution ahead of the crack tip [34], it is straightforward to obtain equation (22):

$$K_{mat}^N = K_{mat} \sqrt{1 + \frac{\rho}{4L}} \quad (22)$$

This equation estimates the apparent fracture toughness ( $K_{mat}^N$ ) from the material fracture toughness ( $K_{mat}$ ), the notch radius ( $\rho$ ) and the critical distance ( $L$ ), and has been widely validated in literature in an extensive range of materials [18,35]. Then,  $K_r$  is given by:

$$K_r = \frac{K_I}{K_{mat}^N} = \frac{K_I}{K_{mat} \sqrt{1 + \frac{\rho}{4L}}} \quad (23)$$

$L$  may be obtained from equation (5) in materials with strictly linear-elastic fracture behavior [18], from experimental testing (e.g., [14,18]), from a combination of experimental testing and finite element simulations (e.g., [14,18]), or through conservative default estimations [36,37]. The validity of equations (22) and (23) is restricted to the validity of the Creager-Paris stress distribution, that is, to slender U-notches (i.e., notches with parallel faces and  $a/\rho \gg 1$ , with  $a$  being the notch length). However, it may be applied to other practical situations, such as V-notches with opening angles below  $90^\circ$ , which have a very similar fracture behavior to U-notches [38]. Additionally, when performing structural integrity assessments, it is important to use material parameters that ensure safe reliable results. This is of particular

**Table 1**  
Summary of the experimental conditions analysed in this research.

Material	Geometry	n	$\rho$ (mm)	E (GPa)	Yield or proof stress (MPa)	$\sigma_u$ (MPa)	$K_{mat,0.05}$ (MPam <sup>1/2</sup> )	L (mm)	$K_I$	$P_L$
S275JR (-120 °C)	CT	23	0–2.0	213	398	613	40.4	0.0137	[4]	[4]
S275JR (-90 °C)	CT	24	0–2.0	211	380	597	61.5	0.0062	[4]	[4]
S275JR (-50 °C)	CT	24	0–2.0	209	349	564	48.4	0.0049	[4]	[4]
S275JR (-30 °C)	CT	24	0–2.0	208	344	548	59.1	0.0061	[4]	[4]
S275JR (-10 °C)	CT	34	0–2.0	207	337	536	74.8	0.0083	[4]	[4]
S275JR (+40 °C)	CT	24	0–2.0	205	331	504	387	0.1697	[4]	[4]
S275JR (+70 °C)	CT	23	0–2.0	203	331	492	599	0.3421	[4]	[4]
S355J2 (-196 °C)	CT	24	0–2.0	218	853	922	29.3	0.0291	[4]	[4]
S355J2 (-150 °C)	CT	21	0–2.0	215	527	759	51.7	0.0084	[4]	[4]
S355J2 (-120 °C)	CT	22	0–2.0	212	459	671	72.0	0.0168	[4]	[4]
S355J2 (-100 °C)	CT	35	0–2.0	212	426	646	93.7	0.0140	[4]	[4]
S355J2 (-50 °C)	CT	24	0–2.0	209	395	602	262	0.0778	[4]	[4]
S355J2 (-20 °C)	CT	24	0–2.0	208	385	587	561	0.3156	[4]	[4]
S460M (-140 °C)	SENB	24	0–2.0	214	702	795	39.8	0.0028	[4]	[4]
S460M (-120 °C)	SENB	24	0–2.0	213	647	758	46.6	0.0075	[4]	[4]
S460M (-100 °C)	SENB	33	0–2.0	212	605	726	56.5	0.0053	[4]	[4]
S690Q (-140 °C)	SENB	24	0–2.0	214	1004	1111	46.2	0.0069	[4]	[4]
S690Q (-120 °C)	SENB	24	0–2.0	213	949	1060	55.9	0.0131	[4]	[4]
S690Q (-100 °C)	SENB	34	0–2.0	212	907	1015	70.1	0.0170	[4]	[4]
Al7075 T651 (LT)	CT	23	0–2.0	71.6	554	612	25.8	0.0150	[4]	[4]
Al7075 T651 (TL)	CT	24	0–2.0	74.4	539	602	25.6	0.0215	[4]	[4]
Al6060 T66	Tubular beam	3	0.8–1.5	70.7	215	264	51.1	0.12	[1]	[1]
PVC	Tubular beam	3	0.8–1.5	3.47	38.6	51.1	6.40	0.08	[1]	[1]
PMMA	SENB	32	0–2.5	3.42	48.5	71.9	1.75	0.105	[4]	[4]
PA6	SENB	25	0–2.0	2.85	54.2	54.2	1.86	0.190	[4]	[4]
ABS <sub>0/90</sub>	SENB	11	0–2.0	2.24	47.7	51.7	1.89	2.68	[4]	[4]
ABS <sub>30/-60</sub>	SENB	11	0–2.0	2.32	59.0	59.3	1.65	2.84	[4]	[4]
ABS <sub>45/-45</sub>	SENB	11	0–2.0	2.38	55.6	60.8	1.87	3.22	[4]	[4]
PLA <sub>0/90</sub>	SENB	19	0–2.0	3.76	51.2	52.0	3.20	0.57	[4]	[4]
PLA <sub>30/-60</sub>	SENB	19	0–2.0	3.31	38.0	42.0	2.91	0.38	[4]	[4]
PLA <sub>45/-45</sub>	SENB	20	0–2.0	2.75	35.3	41.1	2.62	0.24	[4]	[4]
PLA <sub>pl</sub>	Plate	39	0.9–1.3	2.75	35.3	41.1	2.62	0.24	[4]	[4]
SGRF <sub>5</sub> -PA6	SENB	25	0–2.0	3.30	66.9	72.0	1.63	0.157	[4]	[4]
SGRF <sub>10</sub> -PA6	SENB	25	0–2.0	3.55	70.1	78.1	1.88	0.168	[4]	[4]
SGRF <sub>30</sub> -PA6	SENB	24	0–2.0	6.45	105	128	4.34	0.261	[4]	[4]
SGRF <sub>50</sub> -PA6	SENB	25	0–2.0	12.6	161	192	8.38	0.599	[4]	[4]
SGRF <sub>10</sub> -PA6(2)	SENB	25	0–2.0	2.00	31.0	63.4	3.59	1.290	[4]	[4]
SGRF <sub>10</sub> -PA6(5)	SENB	23	0–2.0	0.95	22.5	47.6	3.46	0.450	[4]	[4]
SGRF <sub>50</sub> -PA6(2)	SENB	25	0–2.0	6.92	63.4	112	7.32	1.438	[4]	[4]
SGRF <sub>50</sub> -PA6(4)	SENB	24	0–2.0	6.20	46.5	92.2	5.23	8.838	[4]	[4]
PLA-Gr <sub>0/90</sub>	SENB	20	0–2.0	4.13	50.5	51.0	2.88	0.85	[4]	[4]
PLA-Gr <sub>30/-60</sub>	SENB	20	0–2.0	4.06	41.0	44.3	3.57	2.28	[4]	[4]
PLA-Gr <sub>45/-45</sub>	SENB	20	0–2.0	3.97	47.5	49.0	4.77	1.11	[4]	[4]
PLA-Gr <sub>pl</sub>	Plate	39	0.9–1.3	3.97	47.5	49.0	4.77	1.11	[4]	[4]
Granite	SENB	41	0–10	45.6	9.0	9.0	1.18	6.04	[60]	[4]
Limestone	SENB	41	0–10	64.1	7.8	7.8	0.71	2.71	[60]	[4]

importance in materials where  $K_{mat}$  presents large scatter, as it is the case of ferritic steels operating within their corresponding ductile-to-brittle transition zone. The validation provided in [35] reveals how equation (22) captures the essence of the notch effect (i.e., it is capable to predict how the average values of the apparent fracture toughness evolve with the notch radius), but also that safe structural integrity assessments require safe values of  $K_{mat}$  to be considered, given that this equation is not able to account for the experimental scatter of the fracture toughness (and the apparent fracture toughness) results. This will be described below, in Section 3.

All this being said, it is important to note that there are other

proposals for the analysis of notches using FADs: Horn and Sherry [29,39], as mentioned above, demonstrated the weak dependence of R6 Option 3 (same as BS7910 Option 3) FAL on the notch radius [29], and affirmed that the notch effect is quantified by the increase in the notch fracture toughness. Their equations for  $K_r$  and  $L_r$  may be consulted in [29], although the notch effect in  $L_r$  is generally very low; Pluvinaige [40] proposed the application of the FAD approach together with the global notch criterion. The coordinate  $K_r$  is defined as the ratio of the notch stress intensity factor ( $K_{I,n}$ ) (obtained by using the volumetric method [40]) to the notch fracture toughness ( $K_{I,n}^c$ ), which is the fracture resistance measured from notched specimens with the same radius as the

defect being analyzed.  $K_p$  and  $K_p^c$  are different than  $K_I$  and  $K_{mat}^N$ , respectively, and their units are  $MPa \cdot m^\alpha$ , where  $\alpha$  is not necessarily equal to 0.5. Additionally, Pluvillage does not contemplate any notch effect in  $L_r$ ; Lastly, Matvienko [41], based on the cohesive zone model, the local fracture criterion and the Creager-Paris notch tip stress distribution, developed specific FADs for notches [41]. For further details on these three alternatives, the reader is referred to the corresponding documents [29,39–41].

### 3. Materials

This section describes the materials and specimens used to provide a complete validation of the FAD-TCD approach. They all have been part of previous experimental programs completed by the author, with the present research providing a homogenous treatment of all the materials and specimens in terms of FAL solutions (BS7910 Option 1 in all cases) and material properties, so that the results are comparable and general conclusions may be obtained. Table 1 gathers the summary of these data, covering material identification, specimen geometry (including the notch radii on each case), number of specimens ( $n$ ), material basic tensile properties (required to apply BS7910 Option 1 FAD), the fracture toughness used in the analysis ( $K_{mat}$ ), the critical distance ( $L$ ), and the  $K_I$  and  $P_L$  solutions used in the analyses.  $K_{mat}$  values, in order to provide comparable results, have been those associated to a 5 % probability of failure,  $K_{mat,0.05}$ . For those materials (steels) operating within the ductile-to-brittle transition region (DBTR), it corresponds to the 5 % tolerance bound (1 T thickness) value provided by the Master Curve (MC) [42], whereas in the other cases, it is obtained (assuming normal distribution) by:

$$K_{mat,0.05} = K_{mat,avg} - 1.645 \cdot \frac{stv(K_{mat})}{\sqrt{n}} \quad (24)$$

$K_{mat,avg}$  being the average value of the fracture toughness experimental results,  $stv(K_{mat})$  being the corresponding standard deviation and  $n$  being the number of experimental results. Details on the different material characterization processes may be found in the references provided below. This consideration about the probability of failure associated to the material fracture toughness is absolutely necessary from a structural integrity point of view: given the scatter observed in fracture toughness (and apparent fracture toughness) tests, which cannot be directly captured by equation (22), it is essential to assume a conservative value of  $K_{mat}$  that ensures safe structural integrity assessments. This work proposes the use of  $K_{mat}$  values associated to a 5 % probability of failure, but other probabilities could be considered. Alternatively, the use of lower envelopes of the experimental apparent fracture toughness results could be used to complete FAD assessments in notched components.

Concerning  $P_L$  solutions, [4] presents plane stress and plane strain solutions for CT and SENB specimens. Here, it is considered that plain strain conditions are achieved when the value of applied  $K_J$  is below the limit given by equation (25) [18]:

$$K_J[\text{plane-strain limit}] = \sigma_y (B/2.5)^{0.5} \quad (25)$$

$K_J$  being the applied crack driving force in stress intensity factor units and  $B$  being the thickness of the specimen. When the applied  $K_J$  in a given specimen is lower than the value provided by equation (25) [8], then it is assumed that plain strains conditions are dominant, and the corresponding  $P_L$  solution is given by equations (26) and (27) for CT and SENB specimens, respectively [4]:

$$P_L = 1.455\eta B b \sigma_f \quad (26)$$

$$P_L = \frac{1.455 B b^2 \sigma_f}{S} \quad (27)$$

$b$  being the length of the remaining ligament,  $S$  being the span in SENB specimens,  $\sigma_f$  being the flow stress (average between the yield strength,  $\sigma_y$ , and the ultimate tensile strength,  $\sigma_u$ ) and  $\eta$  following equation (28):

$$\eta = \sqrt{\left(\frac{2a}{b}\right)^2 + \frac{4a}{b} + 2} - \left(\frac{2a}{b} + 1\right) \quad (28)$$

$a$  being the defect size.

Alternatively, here, when  $K_J$  is higher than the limit established by equation (29) plane stress conditions are dominant, and  $P_L$  solutions are provided by equations (30) and (31), respectively, for CT and SENB specimens:

$$K_J[\text{plane-stress onset}] = \sigma_y (\pi B)^{0.5} \quad (29)$$

$$P_L = 1.072\eta B b \sigma_f \quad (30)$$

$$P_L = \frac{1.072 B b^2 \sigma_f}{S} \quad (31)$$

Finally, in those situations located between plane strain and plane stress conditions (equations (25) and (29)),  $P_L$  solution is obtained here by linear interpolation between equations (26) and (30) for CT specimens, or between equations (27) and (31) for SENB specimens.

At this time, it is important to note that equations (25) and [29] rely on  $K_J$ , and not on  $K_I$  as proposed in [18], given that the specimens analyzed in this work do not always meet linear-elastic fracture behavior, on which considering  $K_I$  (which is a particular case of  $K_J$ ) would be enough to complete fracture analyses.  $K_J$ , on the contrary, also works in materials with non-negligible plastic behavior at fracture, as is the case of the structural steels operating within their DBTR or within their upper shelf region, where the plastic component is not negligible and may even be dominant.

The materials and specimens involved in the analyses are the following:

- Steel S275JR: 176 CT specimens, 25 mm thick (1 T), containing U-shaped notches with six different notch radii (0, 0.15, 0.25, 0.50, 1.0 and 2.0 mm). Details on the specimen geometry, mechanical properties (including  $L$ ) and experimental procedures may be found in [15,16,43–45], and are summarized in Table 1. The specimens were tested at five different temperatures, covering the lower shelf ( $-120$  °C,  $-90$  °C), the ductile-to-brittle transition region ( $-50$  °C,  $-30$  °C,  $-10$  °C) and the upper shelf ( $+40$  °C and  $+70$  °C), with the reference temperature ( $T_0$ ) [46] being  $-26$  °C. The experimental critical loads for each individual specimen may be found in [15,16,43–45].
- Steel S355J2: 150 CT specimens, 25 mm thick (1 T), containing U-shaped notches with six different notch radii (0, 0.15, 0.25, 0.50, 1.0 and 2.0 mm). Again, details on the specimen geometry, mechanical properties (including  $L$ ) and experimental procedures may be found in [15,16,43–45] (see the summary in Table 1). In this case, the specimens were tested at six different temperatures, covering the lower shelf ( $-196$  °C), the DBTR ( $-150$  °C,  $-120$  °C,  $-100$  °C), and the upper shelf ( $-50$  °C and  $-20$  °C),  $T_0$  being  $-133$  °C. The experimental critical loads for each individual specimen may be found in [15,16,43–45].
- Steel 460 M: 81 SENB specimens, 15 mm thick (0.6 T), containing U-shaped notches with six different notch radii (0, 0.15, 0.25, 0.50, 1.0 and 2.0 mm). Details on the specimen geometry, mechanical properties (including  $L$ ), experimental procedures and experimental critical loads may be found in [44,47] (see also Table 1). The specimens were tested at three different temperatures within the DBTR ( $-140$  °C,  $-120$  °C,  $-100$  °C),  $T_0$  being  $-91.8$  °C. The value of  $K_{mat,0.05}$  shown in Table 1 corresponds to 1 T equivalent. Therefore, and considering that within the DBTR the toughness depends on the

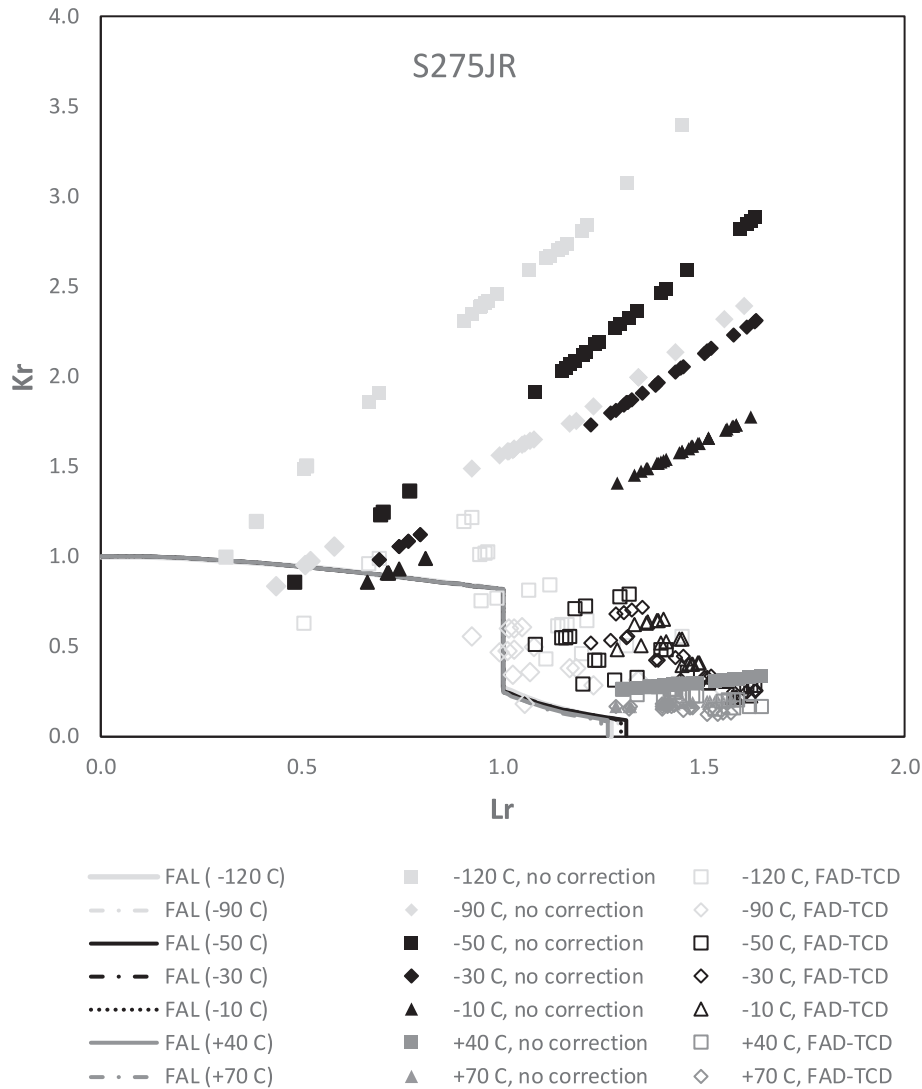


Fig. 2. FAD assessments of steel S275JR specimens at different temperatures (from  $-120\text{ }^{\circ}\text{C}$  up to  $+70\text{ }^{\circ}\text{C}$ ).

thickness, the FAD assessment shown below requires corrections to obtain 0.6 T values. This correction is made through the equation proposed in ASTM E1921 [46]:

$$K_{mat(x)} = 20 + [K_{mat(25mm)} - 20] \cdot \left(\frac{25}{B_x}\right)^{1/4} \quad (32)$$

$K_{mat(x)}$  being the value of  $K_{mat}$  for a specimen thickness of  $B_x$  (15 mm, in this case).

- Steel 690Q: 82 SENB specimens, 15 mm thick (0.6 T), containing U-shaped notches with six different notch radii (0, 0.15, 0.25, 0.50, 1.0 and 2.0 mm). Details on the specimen geometry, mechanical properties (including L), experimental procedures and experimental critical loads may be found in [44,47] (and in Table 1). The specimens were tested at three different temperatures within the DBTR ( $-140\text{ }^{\circ}\text{C}$ ,  $-120\text{ }^{\circ}\text{C}$ ,  $-100\text{ }^{\circ}\text{C}$ ),  $T_0$  being  $-110.8\text{ }^{\circ}\text{C}$ .
- Al7075 T651: 47 CT specimens, 20 mm thick, containing U-notches. The specimens have two distinct orientations, namely LT and TL, and 6 different notch radii (0 mm, 0.15 mm, 0.21 mm, 0.47 mm, 1 mm and 2 mm). Details on geometry, material properties and experimental critical loads may be found in [48].
- Al6060-T66: 3 tubular cantilever beams containing through-thickness circumferential U-notches. The outer diameter varies between 260 mm and 312 mm, the thickness varying between 5 mm and 6 mm and with two possible notch radii: 0.8 mm and 1.5 mm. Details on geometry, material properties and experimental critical loads may be found in [49].
- PVC: first polymer on the list. In this case, 3 tubular cantilever beams containing through-thickness circumferential U-notches were tested. The outer diameter varies between 200 mm and 315 mm, the thickness varied between 3.7 mm and 6.8 mm and, again, with 0.8 mm and 1.5 mm as the two possible notch radii. Details on geometry, material properties and experimental critical loads may be found in [49].
- PMMA: 32 SENB U-notched specimens, 5 mm thick, with notch radii varying from 0 mm up to 2.5 mm. Further details may be found in [14].
- PA6: 27 SENB U-notched specimens, 4 mm thick, made by injection moulding. Notch radii varies from 0 mm up to 2.0 mm. Details may be found in [50,51].
- ABS: in this case, 33 SENB U-notched specimens were made by Fused Filament Fabrication (FFF), covering notch radii from 0 mm up to 2.0 mm and three different raster orientations: 0/90, 30/-60,45/-45. These materials are here referred to as  $\text{ABS}_{0/90}$ ,  $\text{ABS}_{30/-60}$  and  $\text{ABS}_{45/-45}$ , respectively. Details may be found in [52,53] and Table 1. The fracture toughness values are derived from the application of linear-elastic ASTM D5045 [25] standard, in spite of the moderate ductility of the materials in the presence of moisture. This leads to

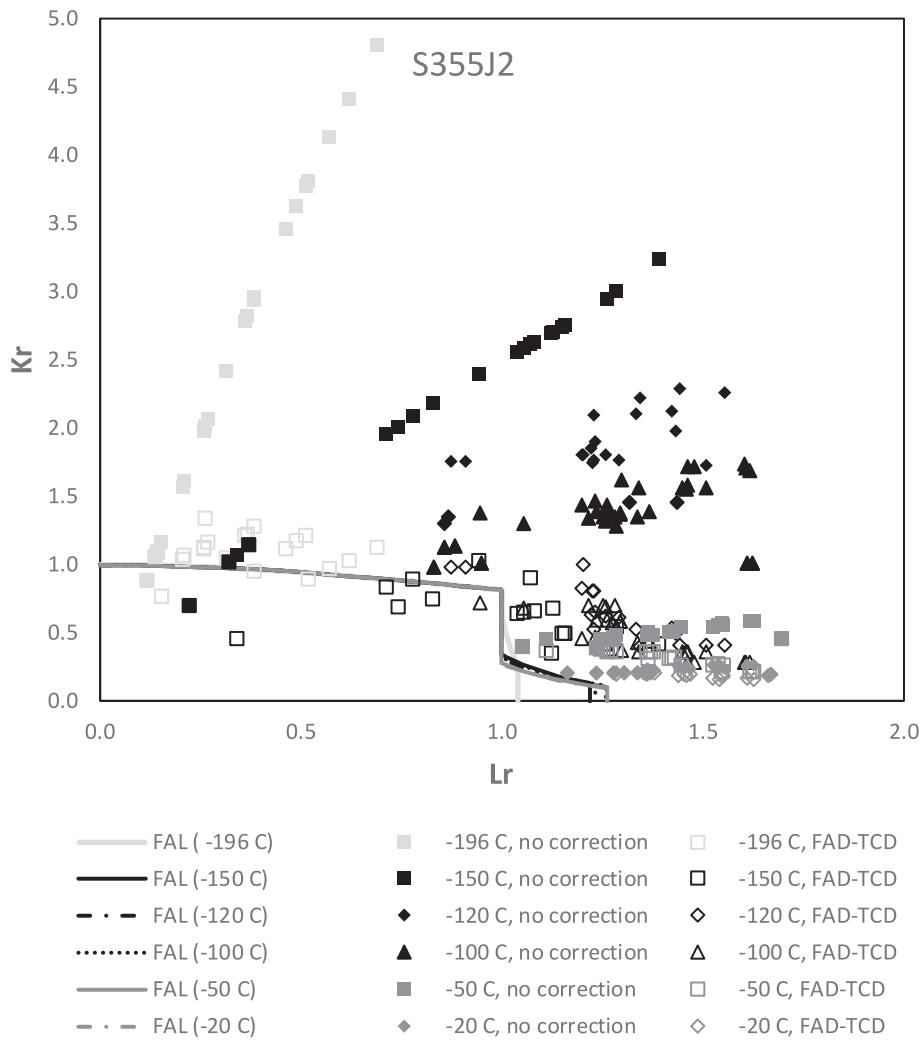


Fig. 3. FAD assessments of steel S355J2 specimens at different temperatures (from  $-196\text{ }^{\circ}\text{C}$  up to  $-20\text{ }^{\circ}\text{C}$ ).

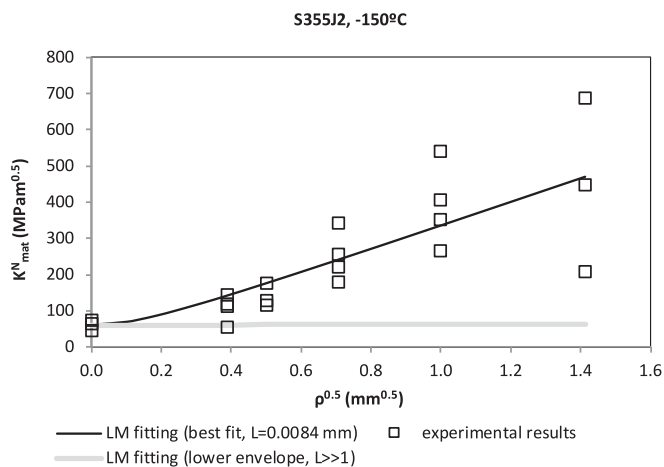


Fig. 4. Fitting process of the apparent fracture toughness results to obtain the value of  $L$  [44].

conservative values of the fracture resistance. The alternative elastic-plastic standard [54] requires the derivation of J-R curves from the measurements of ductile crack propagation, and this was not straightforward in the specimens being analyzed. Moreover, [52,53] presents elastic-plastic estimations of the fracture resistance,

assuming a single value of  $J$  (or  $K_I$ ) at fracture onset and no previous stable (ductile) tearing, but this has been judged here as a non-conservative practice in the context of structural integrity assessments, as demonstrated in [53].

- PLA: 58 SENB U-notched specimens made by Fused Filament Fabrication (FFF), covering notch radii from 0 mm up to 2.0 mm and, again, three different raster orientations (0/90, 30/-60,45/-45), corresponding to PLA<sub>0/90</sub>, PLA<sub>30/-60</sub> and PLA<sub>45/-45</sub>, respectively (see Table 1). Details may be found in [55]. The fracture toughness values are derived from the application of linear-elastic ASTM D5045 [25] standard, for the same reasons mentioned for ABS material.
- Additionally, 39 PLA plates (referred to as PLA<sub>pl</sub>) were printed with raster orientation 45/-45, with machined U- and V-shaped notches and nominal notch radii of 0.9 and 1.3 mm. All the V-notches have an opening angle of 60°, so they have been assumed to behave as U-notches [38], applying the notch correction described above. Details on the PLA plates are available in [56].
- SGFR<sub>x</sub>-PA6: first composite on the list. Short glass fibre reinforced (SGFR) polyamide 6 with four different contents of reinforcement, 5 wt%, 10 wt%, 30 wt% and 50 wt%. These materials are here referred to as SGFR<sub>5</sub>-PA6, SGFR<sub>10</sub>-PA6, SGFR<sub>30</sub>-PA6 and SGFR<sub>50</sub>-PA6, respectively. There are around 25 SENB U-notched specimens, 4 mm thick, per fibre content, all of them obtained through injection moulding, notch radii varying from 0 mm up to 2.0 mm. Further details may be found in [50,51], with a summary of the main

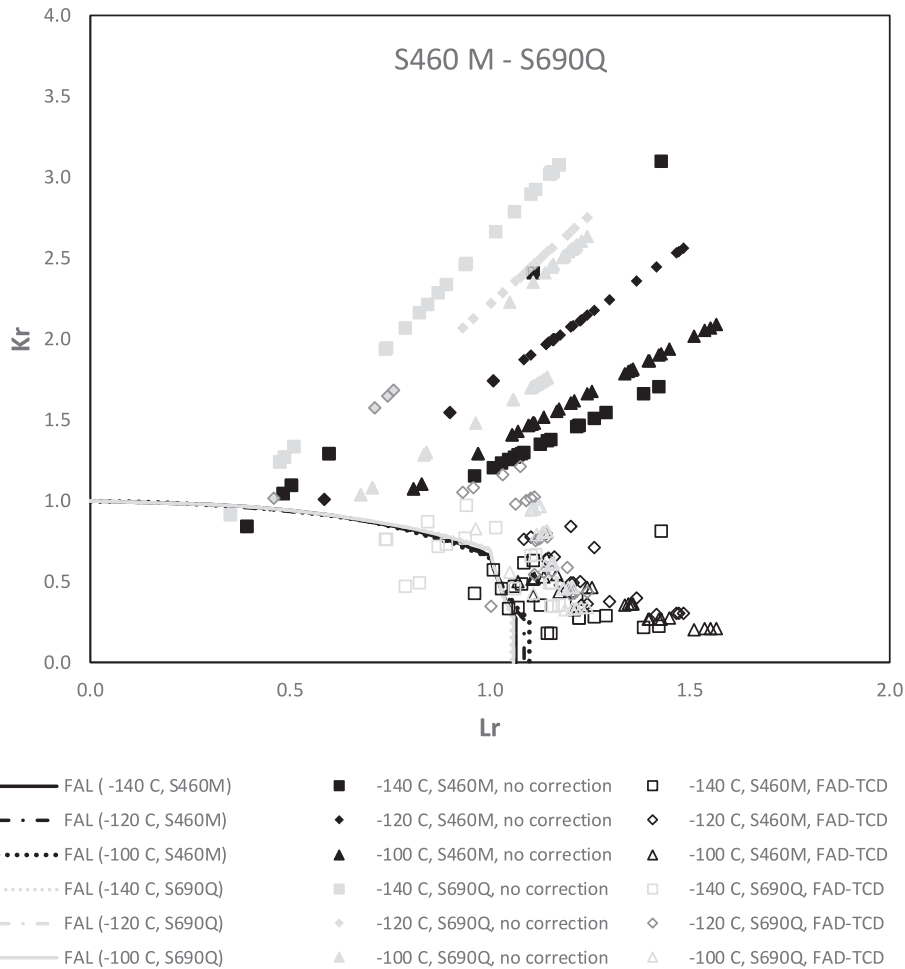


Fig. 5. FAD assessments of steels S460M and S690Q specimens at different temperatures (from  $-140$  °C up to  $-100$  °C).

geometrical and mechanical parameters being gathered in Table 1. In all cases, the materials were dried, with no moisture.

- SGFRx-PA6( $M_c$ ): these materials refer to SGFR-PA6 with x wt.% of SGF and a moisture content of  $M_c$  wt.%. Looking at Table 1, it is straightforward to derive that moisture contents are 2 wt% and 5 wt% for SGFR<sub>10</sub>, and 2 wt% and 4 wt% (saturated) for SGFR<sub>50</sub> materials. There are, therefore, four material conditions, with 97 SENB U-notched specimens, 4 mm thick. Details in [57] and Table 1. The fracture toughness values are derived from the application of linear-elastic ASTM D5045 [25] standard.
- PLA-Gr: 60 SENB U-notched specimens made of graphene reinforced PLA by Fused Filament Fabrication (FFF), covering notch radii from 0 mm up to 2.0 mm and. The content of graphene is fixed at 1 wt%. As in the case of PLA, there are three different raster orientations (0/90, 30/-60,45/-45), corresponding to PLA-Gr<sub>0/90</sub>, PLA-Gr<sub>30/-60</sub> and PLA-Gr<sub>45/-45</sub>, respectively. Details may be found in [55] and in Table 1. The fracture toughness values are derived from the application of linear-elastic ASTM D5045 [25] standard.
- Furthermore, 39 PLA-Gr plates (referred to as PLA-Gr<sub>pl</sub>) were also fabricated with raster orientation 45/-45, including machined U- and V-shaped notches and nominal notch radii of 0.9 mm and 1.3 mm. V-notches (with an opening angle of 60°) are treated here as U-notches. See [58] for details on the PLA-Gr plates.
- Granite: first rock on the list. 41 SENB specimens, tested in 4 point-bending conditions. Notch radii varied between 0.15 mm and 10 mm. Details available in [59], with a summary of the main geometrical and mechanical parameters being shown in Table 1.

- Limestone: As in the case of the granite, 41 SENB specimens were tested in 4 point-bending conditions, with notch radii varying between 0.15 mm and 10 mm. Details available in [59] and Table 1.

With all this, 1,106 specimens made of metallic, polymeric, composite and rock materials, and combining different geometries, notch radii, testing temperatures, and/or fabrication procedures and conditions will be analyzed here through the FAD-TCD approach. In all cases, the notch correction derived from the Line Method (in combination with Creager-Paris stress distribution), the material fracture toughness associated to a 5% failure probability (5% tolerance bound,  $K_{mat,0.05}$ ), and the BS7910 Option 1 FAL will be used.

#### 4. Results and discussion

This section presents the FAD analyses of the 1,106 specimens. For the sake of simplicity, and to avoid an excessive number of FADs, results have been grouped accordingly. In all cases, each specimen is measured without any notch correction (i.e., evaluation as crack-like assessments) and after applying the FAD-TCD correction described above.

Fig. 2 shows the results obtained for steel S275JR at the different temperatures applied, covering lower shelf, DBTR and upper shelf (176 specimens). Overall, it is evident that most of the assessment provides safe estimations, as the assessment point (which represent the specimens at failure) is correctly located in the unacceptable area. There are just a few exceptions (11 assessment points) that predict acceptable situations in specimens that are actually failing. These 11 assessment points correspond to 8 specimens, given that 3 of the specimens with unsafe

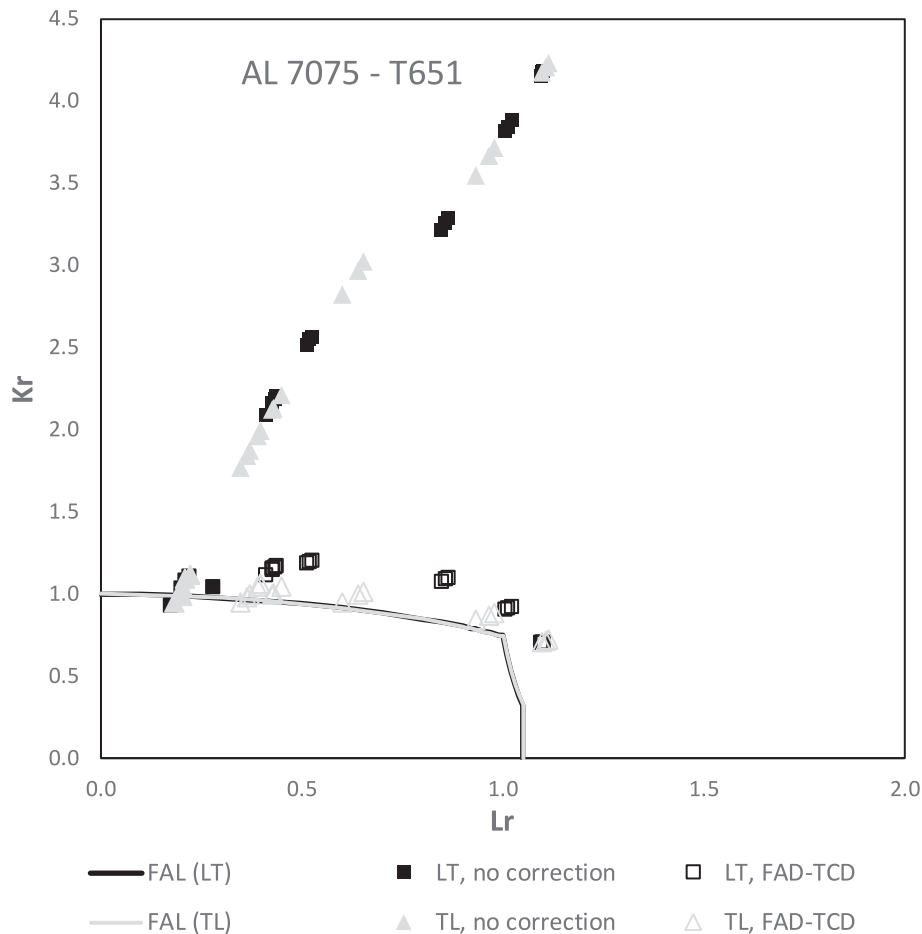


Fig. 6. FAD assessments of aluminium alloy Al7075-T651 (LT and TL orientations).

predictions are cracked, and their corresponding two assessment points (with and without notch correction) are coincident. Thus, 8 out of 176 specimens (4.5 %) are providing unsafe predictions, which is reasonable considering that the  $K_{mat,0.05}$  value used in the assessments is associated with a 5 % probability of failure. Moreover, ignoring the 29 cracked specimens, there are 5 unsafe results out of 147 (3.4 %) notched specimens, again in concordance with the fracture toughness value considered in the assessments.

Additionally, and looking at the assessment points without any notch correction, for a given temperature, the evaluation points follow a straight line (as the defect length is the same or very similar in all specimens), with the closest points to the FAL corresponding to the cracked specimens. These points move away from the FAL as the notch radius increases. Besides, the slope of the lines is smaller the higher the temperature, given that the behavior of the material tends to be more ductile. Finally, once the notch correction is applied, the assessment points are vertically displaced, approaching to the FAL and reducing the conservatism (which is greater the further the point is from the FAL). Summarizing, the FAD-TCD correction, for steel 275JR, provides safe assessments and reduces the conservatism.

One final observation is that the corresponding FALs (one per temperature) are basically coincident, with small differences at the cut-off ( $L_{r,max}$ ).

Fig. 3 shows the results obtained in steel S355J2. As in the previous case, the assessment of the (150) different specimens is performed without and with (FAD-TCD) notch correction. Here, 12 assessments provide unsafe predictions, as they represent the specimens at failure but are evaluated as acceptable. The 12 points correspond to 10 specimens, given that 2 of the specimens are cracked and, thus, their

assessment points without and with notch correction are coincident. Consequently 10 specimens out of 150 (6.6 %) generate unsafe predictions, again something rational considering the value of fracture toughness ( $K_{mat,0.05}$ ) assumed in the assessments. When cracked specimens are not considered, 8 out of 125 specimens (6.4 %) provide unsafe predictions. Interestingly, there is a point representing a CT specimen with a notch radius of 0.15 mm and tested at  $-150$  °C (black open square symbol) that provides a significant level of unsafety, as it is located well within the acceptable area. In order to explain this type of results, two points must be considered: first, the inherent high scatter of fracture results within the DBTR, which is conveniently addressed by the Master Curve. However, by considering the 5 % tolerance bound, that percentage of results could approximately provide unsafe evaluations; secondly, when dealing with the LM notch correction itself (equations (22) and (23)), the value of  $L$  used in this work for the different steels has been derived from the best fit of equation (22) to the experimental measurements of  $K_{mat}^N$  (see [44] for details). Now, looking at the fitting of the results for a 0.15 mm notch radius and  $-150$  °C, it can easily be observed that the LM prediction is, in some cases, overestimating the notch effect, as shown in Fig. 4 ([44]). This kind of situations, where the number of experimental results is limited, the scatter on fracture toughness results is very high, and the LM predictions tend to overestimate the notch effect for a particular notch radius, can be easily avoided by considering larger values of  $L$  that provide a lower envelope of the whole set of experimental results. However, in this case (see Fig. 4), this would make it necessary to basically neglect the notch effect for these particular conditions of material and testing temperature, as the lower value of apparent fracture toughness obtained for a notch radius of 0.15 mm is slightly lower than the average value obtained in

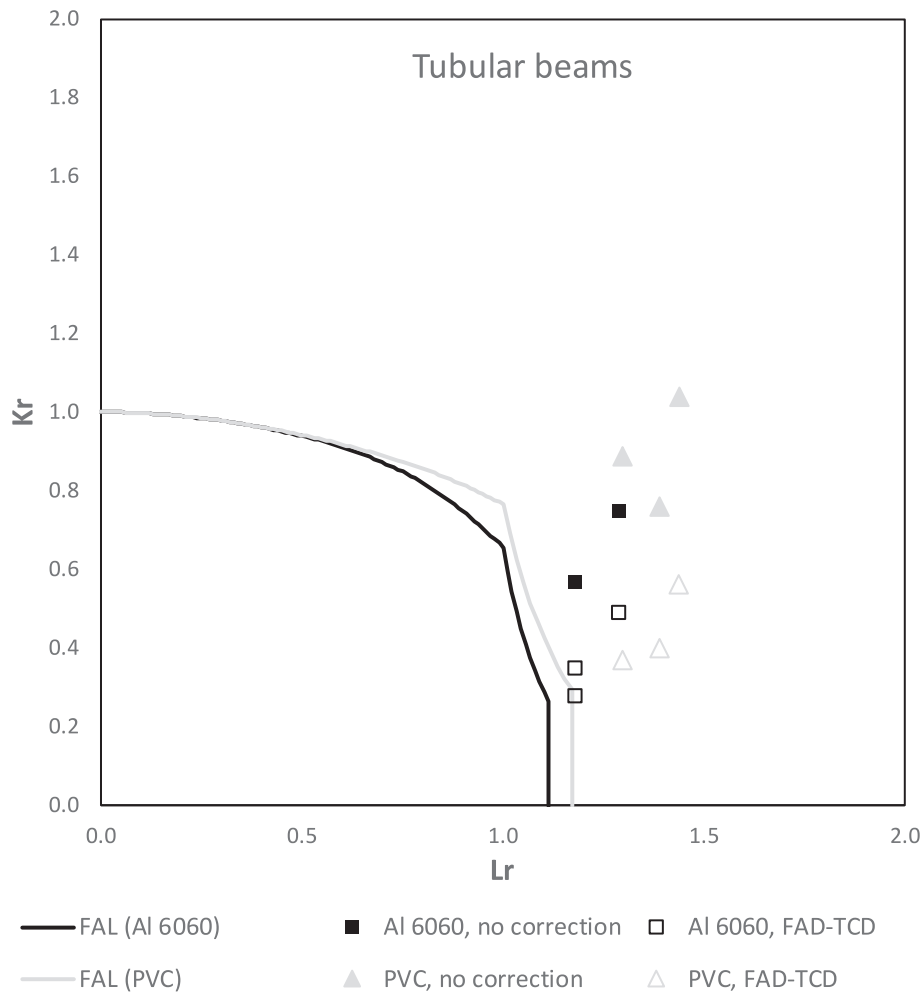


Fig. 7. FAD assessments of tubular beams (Al6060-T66 and PVC).

cracked conditions. In other words, in this particular case, the assessment of notched specimens using the lower envelope fitting would coincide without and with notch correction. Engineering judgement may, therefore, be required for a practical application of the approach, depending on factors such as the scatter of the observed results or the criticality of the component being assessed, among others.

Finally, it is worth mentioning that the corresponding FALs (one per temperature) are basically coincident, with small differences at the cut-off ( $L_{r,max}$ ), except for the FAL at  $-196\text{ }^{\circ}\text{C}$ , whose cut-off occurs at a much lower value of  $L_{r,max}$ . This is a direct consequence of a much lower hardening behavior of the material at this temperature.

Fig. 5 presents the results obtained in steels S460M and S690Q, both with continuous yielding tensile curves. All the specimens were tested within their corresponding DBTR. In this case, 13 assessments provide unsafe predictions, with the specimens at failure being evaluated as acceptable. The 13 points correspond to 11 specimens, given that 2 of the specimens are cracked and, thus, their assessment points without and with notch correction are coincident. Accordingly, 11 specimens out of 163 (6.7 %) generate unsafe predictions, which is in concordance with the fracture toughness ( $K_{mat,0.05}$ ) considered in the assessments. When cracked specimens are not considered, 9 out of 136 specimens (6.6 %) provide unsafe predictions. Looking into the results providing unsafe predictions, most of them correspond to S690Q specimens tested at  $-140\text{ }^{\circ}\text{C}$ , with some cases of S460M tested at the same temperature. The reason for these results is exactly the same as that explained above for steel S355J2: the corresponding values of  $L$  used in the analyses have been derived from the best fit of equation (22) to the experimental

measurements of  $K_{mat}^N$ , and this causes an overestimation of the notch effect for certain notch radii (from 0.15 mm to 0.5 mm in the case of steel S690Q). In [47] the reader may find similar graphs to that shown in Fig. 4.

All this being said, it is clear how the assessment points corresponding to the FAD-TCD assessments generally provide safe predictions with a much lower level of conservatism (i.e., the points are above the FAL and much closer to it than the points without notch correction).

Fig. 6 presents the results obtained in Al7075-T651 alloy. In this case, the notch correction is particularly effective: the assessment of the notched specimens without any notch correction leads to increasingly conservative results (i.e., the larger the radius the larger the conservatism), with some of the assessment points being located significantly far from the FAL. However, when applying the notch correction, the assessment points are located very close to the FAL, providing an assessment which is very close (yet conservative) to the real physical fracture. There are 5 assessments out of 94 (5.3 %) generating slightly non-conservative results, four of them corresponding to two cracked specimens. Thus, focussing on notched specimens, just 1 out of 36 (2.7 %) has provided a very slightly non-conservative evaluation when applying the notch correction. The results in Al7075-T651 alloy are, therefore, very accurate and still safe.

Fig. 7 presents the results on two very different materials (Al 6060-T66 and PVC). Their assessments have been grouped together given that they correspond to real structural components (commercial tubes working as cantilever beams) with a through-thickness crack close to the structural support (see [49] for details). The results show how the initial

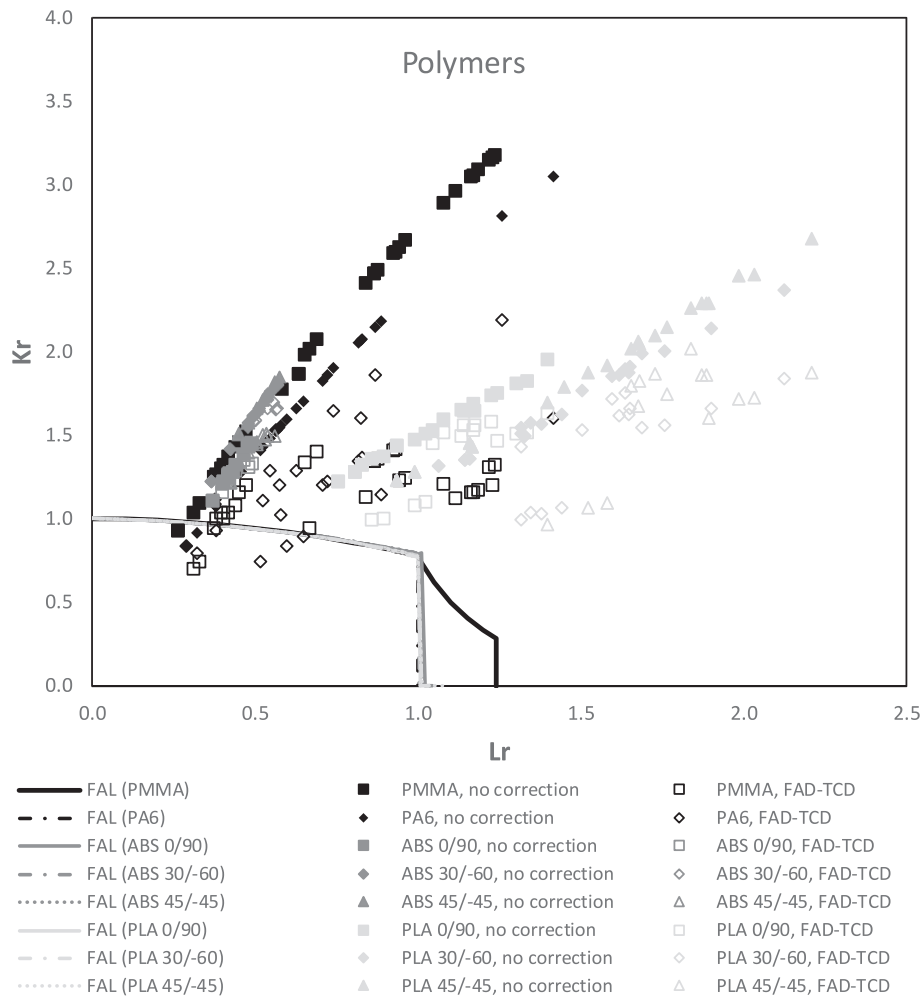


Fig. 8. FAD assessments of polymers PMMA, PA6, ABS and PLA. ABS and PLA are FFF materials with three different raster orientations.

level of conservatism is much more moderate than that generally found in the previous CT and SENB specimens, but the notch correction still improves the accuracy (i.e., assessment points closer to the corresponding FAL) yet providing safe results. The different nature of the two materials is also evident looking at their corresponding FALs.

Fig. 8 presents the results obtained in the different polymers involved in the analysis, with 148 SENB specimens. It covers PMMA, injection moulded PA6, and FFF ABS and PLA (both with 3 different raster orientations). There are 12 assessments providing unsafe estimations, 4 of which correspond to (2) cracked specimens. Thus, focussing on the 119 notched specimens (i.e., 29 are cracked), there are 7 whose evaluation through the FAD-TCD approach is unsafe, corresponding to a still reasonable 5.8 %. One of the notched specimens, with notch radius of 0.25 mm and close to a crack-like defect, provides an unsafe assessment even when treated as a crack (thus, this specimen is associated to two unsafe predictions). Overall, again, the assessment points after the FAD-TCD correction are closer to the FAL, providing lower conservatism and generally safe evaluations. Interestingly, the FFF materials tend to provide the higher level of conservatism for the two types of evaluations (without and with notch correction).

Fig. 9 gathers the results corresponding to the different SENB specimens made of composite materials, covering injection moulded SGFR-PA6, with different contents of short glass fibre and moisture, and FFF PLA-Gr, with 3 different raster orientations and a fixed content of graphene (1 wt%). In total, there are 256 SENB specimens evaluated in the FADs, with and without notch correction. The results show 13 assessment points providing unsafe predictions, 10 of which correspond to 5

specimens containing crack-like defects, and 3 corresponding to 2 notched specimens. As in the case of polymers, one of the notched specimens, with notch radius of 0.25 mm, provides an unsafe assessment even when treated as a crack. In other words, 7 out of 256 specimens (2.7 %) generate unsafe results. When dealing with notched specimens, 2 out of 205 (less than 1 %) are unsafely evaluated when applying the FAD-TCD approach. The results reveal the suitability of the methodology in evaluating these composites, with a number of unsafe predictions well below the tolerance bound selected for the material fracture toughness (5 % probability of failure), and with the assessment points when applying the notch correction being much closer to the FAL than those obtained when there is no correction at all. The improvement in the accuracy is particularly significant in the case of SGFR-PA6 without moisture. Also, as in the case of polymers, the FFF material presents the higher level of conservatism (without and with notch correction).

Fig. 10 gathers the results on (FFF) 3D printed plates made of PLA and PLA-Gr, comprising a very different type of geometry when compared to SENB (and CT) specimens, and including both U- and V-notches. The raster orientation is fixed for all the plates (45/-45). For the sake of consistency, the fracture toughness values of the two materials are the same as those used above for the analysis of the SENB specimens, which were derived from ASTM D5045 standard. The results show a high level of conservatism even when the notch correction is applied, with all the 156 assessments (78 as crack-like defects and 78 with notch corrections) providing safe results. The FAD-TCD approach improves the predictions, often just slightly, maintaining a high level of safety. These results are reasonable considering that the SENB specimens made of

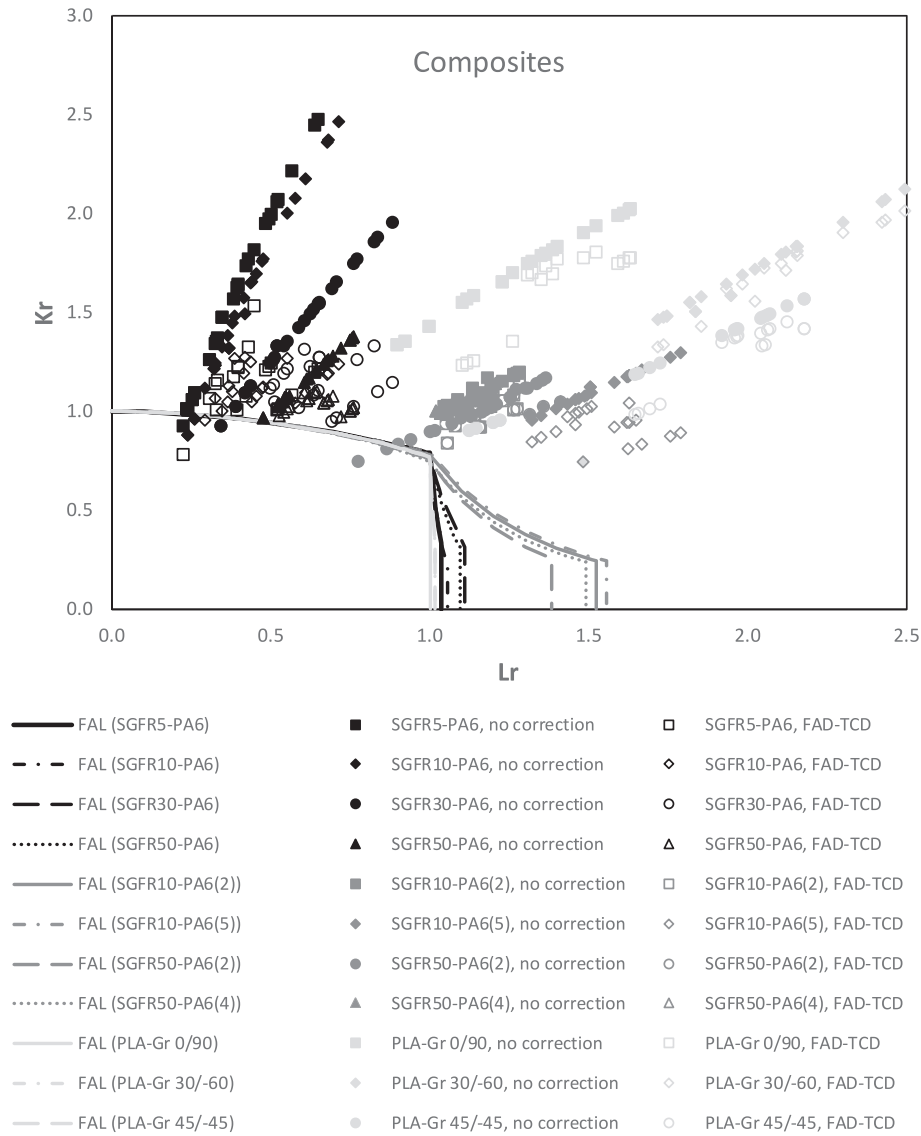


Fig. 9. FAD assessments of SGFR and PLA-Gr composites. SGFR materials combine different amounts of GF and moisture; (FFF) PLA-Gr composites include three different raster orientations.

these materials already presented significant conservatism. The plates, which are subjected to pure tensile loading and (part of them) have low  $a/W$  ratio (0.25), are subjected to lower levels of constraint, thus providing even more conservative results than the fracture mechanics traditional high-constrained specimens.

Fig. 11 gathers the results for the 82 SENB specimens made of granite and limestone. All the 164 predictions are safe, with the notch corrections being moderate as a consequence of the high values of  $L$  presented by these two materials.

Finally, Fig. 12 shows the 2,212 assessments of the 1,106 specimens. Here, the different materials are not distinguished. The aim is to provide experimental evidence about the safety of the FAD-TCD approach and its increasing level of accuracy when compared with the assessment of notches as if they were crack-like defects. Given that BS7910 Option 1 FAL is material-dependent, it has been necessary to use a FAL that is not material-dependent. Given that the current version of BS7910 does not have such an option, FITNET FFS Option 0 [61] has been used. For materials with discontinuous yielding, it follows equations (33) to (34):

$$K_r = f(L_r) = \left[ 1 + \frac{1}{2}(L_r)^2 \right]^{-1/2} \quad L_r \leq 1 \quad (33)$$

$$K_r = f(L_r) = 0 \quad L_r > 1 \quad (34)$$

For materials with continuous yielding, and considering the conservative assumption that there is no hardening (i.e.,  $L_{r,max} = 1$ , thus avoiding the material dependence related with the hardening capacity), it follows equations (34) and (35):

$$K_r = f(L_r) = \left[ 1 + \frac{1}{2}(L_r)^2 \right]^{-1/2} \cdot \left[ 0.3 + 0.7 \cdot e^{-0.6 \cdot (L_r)^6} \right] \quad L_r \leq 1 \quad (35)$$

It is straightforward to see that equation (35) provides a more conservative FAL. With the aim of simplifying Fig. 12, providing a unique FAL for the different materials (some having continuous yielding, others having continuous yielding and others basically without any yielding), equations (34) and (35) have been used.

Overall, it is evident how the notch correction provides more physically consistent results, with the assessment point much closer to the FAL, yet maintaining a high level of safety. There are 66 unsafe assessments out of 2212 (less than 3%), 32 of which correspond to 16 cracked

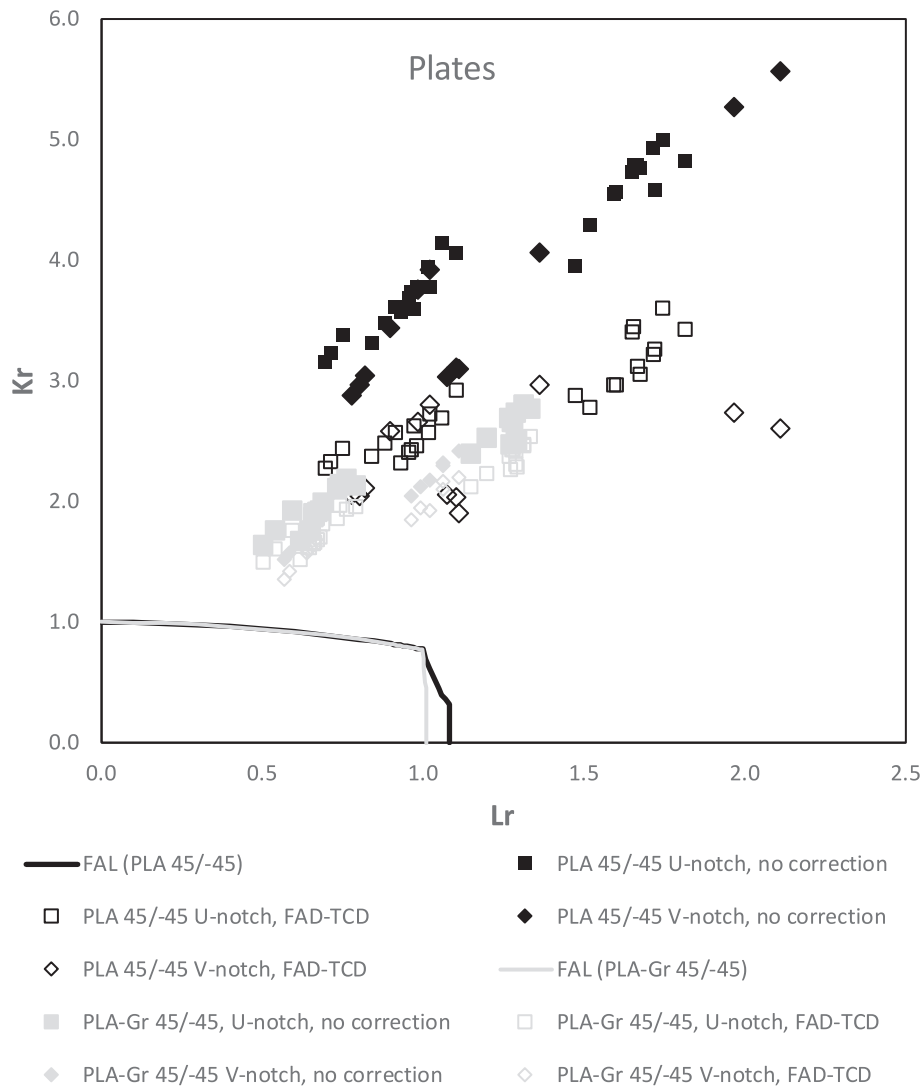


Fig. 10. FAD assessments of PLA and PLA-Gr plates. Raster orientation 45/-45.

specimens (as explained above, cracked specimens provide two coincident assessment points, given that the notch correction is null and the assessment point representing the assessment with notch correction is exactly the same as that obtained with a crack-like assessment). Thus, focussing on notched specimens, there are 32 notched specimens out of 895 (less than 3.5 %) unsafely evaluated through the FAD-TCD approach, and generating 34 unsafe predictions (two of the specimens generate two unsafe predictions each, one of them even when they are treated as cracks). These results are in very good concordance with the 5 % probability of failure assumed for the material fracture toughness  $K_{mat}$ .

When using the FAD methodology to analyze components containing defects, the obtained conservatism associated to a component represented at fracture conditions may be estimated by (see Fig. 1, assessment point B):

$$CF = \frac{\overline{OB}}{\overline{OP}} \quad (36)$$

where here, CF stands for Conservatism Factor. If  $CF > 1$ , the result is conservative;  $CF = 1$  when the assessment is exact, and;  $CF < 1$  when the assessment is unsafe (non-conservative). As mentioned above, the analysis performed above with the corresponding notch correction reduces the conservatism significantly. In order to check how much this

conservatism is reduced, one could calculate the CF for each combination of material type, material condition, defect type, notch radius, specimen geometry, etc., comparing the CF obtained without and with notch correction. Here, in order to simplify the process and to simply obtain a reference value of how much the CF is reduced when applying the FAD-TCD approach to 1,106 specimens combining a number of different situations, the average ( $K_r$ ,  $L_r$ ) coordinates of the 2,212 evaluations (1,106 without correction, 1,106 with FAD-TCD correction) have been calculated, the resulting points being represented in Fig. 1. Point A represents the average coordinates (1.06, 1.67) of the fracture assessments of the 1106 specimens without any notch correction (i.e., crack-like assessment), whereas Point B represents the average coordinates (1.06, 0.99) of the 1106 specimens evaluated through the FAD-TCD approach. The resulting CF (when using FITNET FFS Option 0, as in Fig. 1) are 1.84 and 1.30, respectively. Thus, the conservatism (excess of CF above 1) is reduced to almost one third of that originally obtained without any correction, yet maintaining a reasonable margin when compared to hypothetical exact evaluations.

## 5. Conclusions

This paper provides a comprehensive FAD analysis of 1,106 fracture tests performed on notched specimens. The assessments, performed homogeneously for all cases, cover very different types of materials

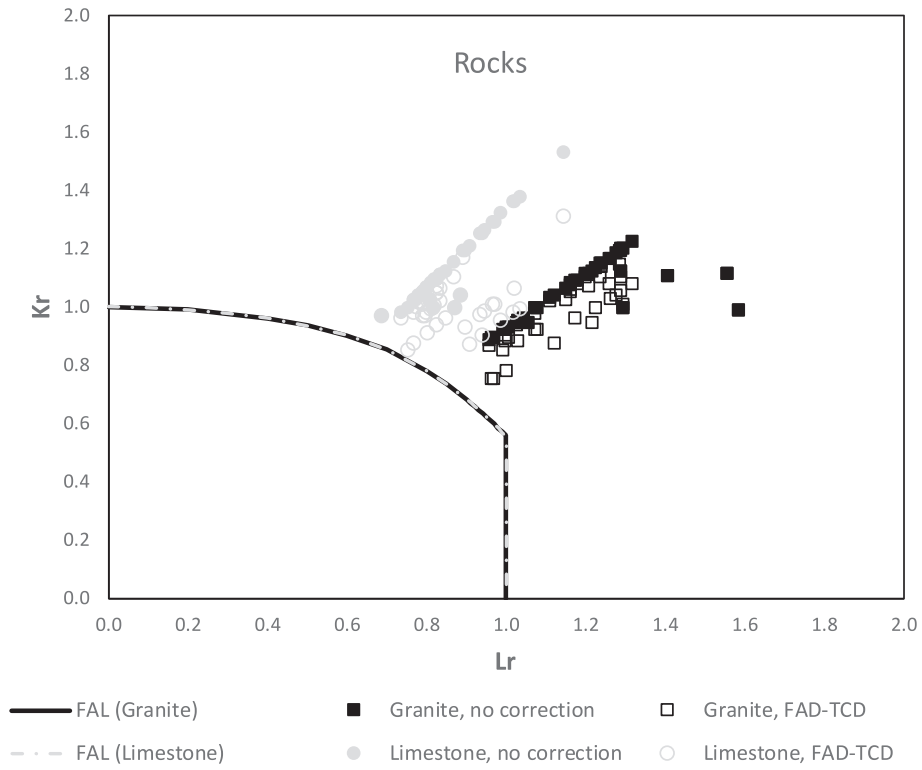


Fig. 11. FAD assessments of granite and limestone.

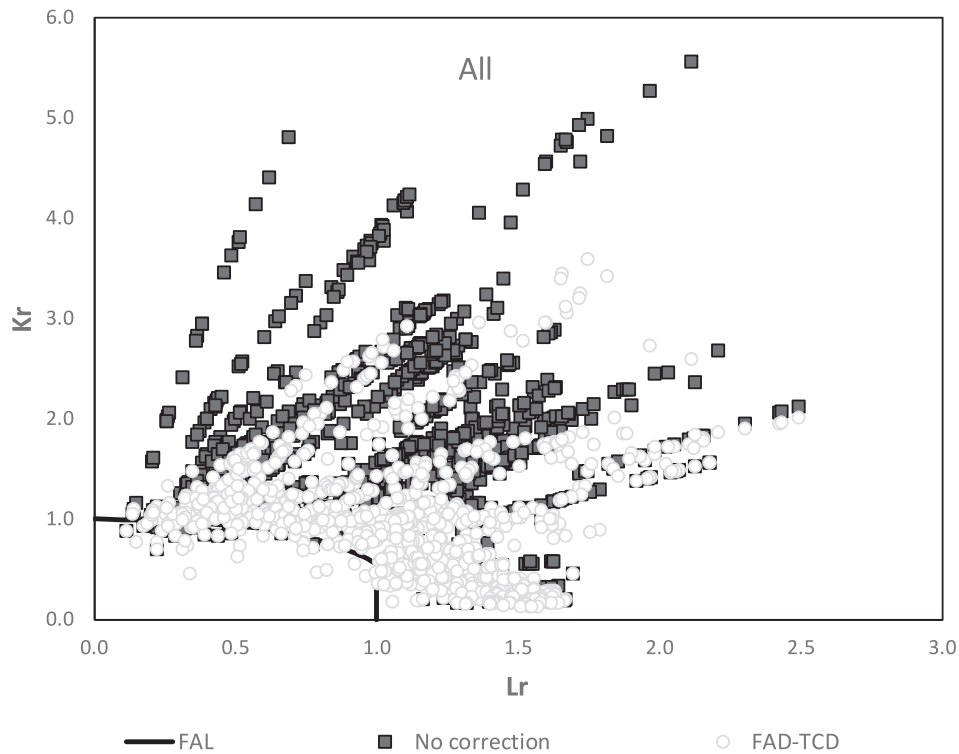


Fig. 12. FAD assessments of all the specimens and materials, without (crack-like assessment) and with FAD-TCD notch correction.

(metals, polymers, composites, rocks), working conditions (e.g., from lower shelf temperatures up to upper shelf temperatures in the case of steels), fabrication methods (e.g., injection moulding vs. FFF in the case of polymers and composites), testing specimens (conventional CT and SENB specimens vs. tubular beams or structural plates) and notch radii

(from 0 mm in crack-like defects up to 10 mm, with the vast majority between 0 mm and 2 mm).

The approach followed, referred to as the FAD-TCD approach, has been theoretically justified, and consists in maintaining the FAL ( $f(L_r)$ ) and limit load ( $P_L$ ) solutions used in the analysis of cracks (well defined

in structural integrity assessment procedures) and applying the notch effect correction on  $K_r$  by considering the apparent fracture toughness estimation derived from the Theory of Critical Distances (particularly, here, from the Line Method).

The application of the FAD-TCD approach to 1,106 specimens, 895 of which have notch radii larger than 0 mm), significantly reduces the conservatism associated to the evaluation of notches as crack-like defects, with the assessment points much closer to the limiting condition defined by the FAL, yet maintaining the safety of the analysis.

#### CRedit authorship contribution statement

**Sergio Cicero:** Writing – original draft, Methodology, Investigation, Funding acquisition, Formal analysis, Data curation, Conceptualization.

#### Declaration of competing interest

The authors declare that they have no known competing financial interests or personal relationships that could have appeared to influence the work reported in this paper.

#### Data availability

The data that support the findings of this study are available from the corresponding author upon reasonable request.

#### Acknowledgements

This publication is part of the project “Comportamiento en fractura y efecto entalla en compuestos de matriz termoplástica obtenidos por fabricación aditiva, PID2021-122324NBI00” funded by MCIN/AEI/10.13039/501100011033/FEDER “Una manera de hacer Europa”.

The author would like to thank the work and collaboration over the years of those who have contributed to his research in notch mechanics, and specially to: Dr. Virginia Madrazo, Dr. Tiberio García, Dr. Pablo González, Dr. Juan Diego Fuentes, Dr. Francisco Tomás, Dr. Borja Arroyo, Dr. José Alberto Álvarez, Dr. Roberto Lacalle, Dr. Federico Gutiérrez-Solana, Dr. Sergio Arrieta and Dr. Marcos Sánchez.

#### References

- [1] BS 7910:2019, Guide to methods for assessing the acceptability of flaws in metallic structures, British Standard Institution, London, 2019.
- [2] API 579-1/ASME FFS-1, Third edition. USA, The American Society of Mechanical Engineers, New York, 2016.
- [3] R6: Assessment of the integrity of structures containing defects, Revision 4, with amendments to Amendment 11, EDF Energy, Gloucester, 2015.
- [4] T.L. Anderson, *Fracture Mechanics: Fundamentals and Applications*, CRC Press, Boca Raton, USA, 2005.
- [5] U. Zerbst, R.A. Ainsworth, K.-H. Schwalbe, Basic principles of analytical flaw assessment methods, *Int. J. Press. Vessel. Pip.* 77 (2001) 855–867.
- [6] S.T. Lie, Z.M. Yang, W.M. Gho, Validation of BS7910:2005 failure assessment diagrams for cracked square hollow section T-, Y- and K-joints, *Int. J. Press. Vessel. Pip.* 86 (2009) 335–344.
- [7] R.A. Ainsworth, A.C. Bannister, U. Zerbst, An overview of the European flaw assessment procedure SINTAP and its validation, *Int. J. Press. Vessel. Pip.* 77 (2000) 869–876.
- [8] K. Kouzoumis, I. Hadley, M. Mostafavi, Validation of BS 7910 fracture assessment procedures; wide plates and cylinders, *Int. J. Press. Vessel. Pip.* 190 (2021) 104309.
- [9] D. Gay, *Composite Materials: Design and Applications*, fourth ed., CRC Press, USA, 2023.
- [10] N.P. Padture, Advanced structural ceramics in aerospace propulsion, *Nat. Mater.* 15 (2016) 804–809.
- [11] T.R. Rashidov, N.A. Nishonov, Seismic behavior of underground polymer piping with variable interaction coefficients, *Soil Mech. Found. Eng.* 53 (2016) 196–201.
- [12] J.D. Fuentes, S. Cicero, F.T. Ibáñez-Gutiérrez, I. Procopio, On the use of British standard 7910 option 1 failure assessment diagram to non-metallic materials, *Fatigue Fract. Eng. Mater. Struct.* 41 (2018) 146–158.
- [13] M. Martínez, A.J. Cano, A. Salazar, J. Rodríguez, On the failure assessment diagram methodology in polyamide 12, *Eng. Fract. Mech.* 269 (2022) 108558.
- [14] S. Cicero, V. Madrazo, I.A. Carrascal, Analysis of notch effect in PMMA by using the Theory of Critical Distances, *Eng. Fract. Mech.* 86 (2012) 56–72.
- [15] S. Cicero, V. Madrazo, T. García, Analysis of notch effect in the apparent fracture toughness and the fracture micromechanisms of ferritic-pearlitic steels operating within their lower shelf, *Eng. Fail. Anal.* 36 (2014) 322–342.
- [16] S. Cicero, V. Madrazo, T. García, J. Cuervo, E. Ruiz, On the notch effect in load bearing capacity, apparent fracture toughness and fracture mechanisms of polymer PMMA, aluminium alloy Al7075-T651 and structural steels S275JR and S355J2, *Eng. Fail. Anal.* 29 (2013) 108–121.
- [17] F.J. Gómez, M. Elices, Fracture loads for ceramic samples with rounded notches, *Eng. Fract. Mech.* 73 (2006) 880–894.
- [18] D. Taylor, *The Theory of Critical Distances: A New Perspective in Fracture Mechanics*, Elsevier, London, 2007.
- [19] F. Berto, P. Lazzarin, Recent developments in brittle and quasi-brittle failure assessment of engineering materials by means of local approaches, *Mater. Sci. Eng. R Rep.* 75 (2014) 1–48.
- [20] M. Allouti, C. Schmitt, G. Pluvinage, Assessment of a gouge and dent defect in a pipeline by a combined criterion, *Eng. Fail. Anal.* 36 (2014) 1–13.
- [21] C.T. Ng, L. Susmel, Notch static strength of additively manufactured acrylonitrile butadiene styrene (ABS), *Addit. Manuf.* 34 (2020) 101212.
- [22] G.C. Sih, Strain-energy-density factor applied to mixed mode crack problems, *Int. J. Fract.* 10 (1974) 305–321.
- [23] S. Cicero, V. Madrazo, I.A. Carrascal, R. Cicero, Assessment of notched structural components using failure assessment diagrams and the theory of critical distances, *Eng. Fract. Mech.* 78 (2011) 2809–2825.
- [24] P. González, S. Cicero, B. Arroyo, J.A. Álvarez, A Theory of Critical Distances based methodology for the analysis of environmentally assisted cracking in steels, *Eng. Fract. Mech.* 214 (2019) 134–148.
- [25] ASTM D5045-14(2022), Standard Test Methods for Plane-Strain Fracture Toughness and Strain Energy Release Rate of Plastic Materials, ASTM International, West Conshohocken, USA, 2022.
- [26] ASTM E1820-23, Standard Test Method for Measurement of Fracture Toughness, ASTM International, West Conshohocken, USA, 2023.
- [27] ASTM C1421-18, Standard Test Methods for Determination of Fracture Toughness of Advanced Ceramics at Ambient Temperature, ASTM International, West Conshohocken, USA, 2018.
- [28] A.G. Miller, Review of limit loads of structures containing defects, *Int. J. Press. Vessel. Pip.* 32 (1988) 197–327.
- [29] A.J. Horn, A.H. Sherry, An engineering assessment methodology for non-sharp defects in steel structures - Part I: procedure development, *Int. J. Press. Vessel. Pip.* 89 (2012) 137–150.
- [30] J. Ruiz Ocejo, F. Gutiérrez-Solana, M.A. González-Posada, Report/SINTAP/UC/06: Structural integrity assessment procedures for European industry (SINTAP), University of Cantabria, Spain, 1998.
- [31] R.A. Ainsworth, F. Gutiérrez-Solana, J. Ruiz Ocejo, Analysis levels with the SINTAP defect assessment procedures, *Eng. Fract. Mech.* 67 (2000) 515–527.
- [32] J. Ruiz Ocejo, F. Gutiérrez-Solana, M.A. González-Posada, Report/SINTAP/UC/08: Structural Integrity Assessment Procedures for European Industry (SINTAP), University of Cantabria, Spain, 1998.
- [33] A.C. Bannister, J. Ruiz Ocejo, F. Gutiérrez-Solana, Implications of the yield stress/tensile stress ratio to the SINTAP failure assessment diagrams for homogeneous materials, *Eng. Fract. Mech.* 67 (2000) 547–562.
- [34] M. Creager, P.C. Paris, Elastic field equations for blunt cracks with reference to stress corrosion cracking, *Int. J. Fract. Mech.* 3 (1967) 247–252.
- [35] S. Cicero, T. García, V. Madrazo, On the Line Method apparent fracture toughness evaluations: Experimental overview, validation and some consequences on fracture assessments, *Theor. Appl. Fract. Mech.* 78 (2015) 15–19.
- [36] J.D. Fuentes, S. Cicero, I. Procopio, Some default values to estimate the critical distance and their effect on structural integrity assessments, *Theor. Appl. Fract. Mech.* 90 (2017) 204–212.
- [37] S. Cicero, J.D. Fuentes, I. Procopio, V. Madrazo, P. González, Critical distance default values for structural steels and a simple formulation to estimate the apparent fracture toughness in U-notched conditions, *Metals* 8 (11) (2018) 871.
- [38] P. Lazzarin, F. Berto, Some expressions for the strain energy in a finite volume surrounding the root of blunt V-notches, *Int. J. Fract.* 135 (2005) 161–185.
- [39] A.J. Horn, A.H. Sherry, An engineering assessment methodology for non-sharp defects in steel structures - Part II: procedure validation and constraint analysis, *Int. J. Press. Vessel. Pip.* 89 (2012) 151–161.
- [40] G. Pluvinage, Pipe-defect assessment based on the limit analysis, failure-assessment diagram, and subcritical crack growth, *Mater. Sci.* 42 (2006) 127–139.
- [41] Y.G. Matvienko, Local fracture criterion to describe failure assessment diagrams for a body with a crack/notch, *Int. J. Fract.* 124 (2003) 107–112.
- [42] K. Wallin, The scatter in  $K_{IC}$ -results, *Eng. Fract. Mech.* 19 (1984) 1085–1093.
- [43] S. Cicero, V. Madrazo, T. García, On the assessment of U-shaped notches using Failure Assessment Diagrams and the Line Method: Experimental overview and validation, *Theor. Appl. Fract. Mech.* 80 (2015) 235–241.
- [44] V. Madrazo, S. Cicero, T. García, Assessment of notched structural steel components using failure assessment diagrams and the theory of critical distances, *Eng. Fail. Anal.* 36 (2014) 104–120.
- [45] S. Cicero, T. García, V. Madrazo, I.A. Carrascal, E. Ruiz, Analysis of notch effect in load bearing capacity, apparent fracture toughness and fracture micromechanisms of ferritic-pearlitic steels, *Eng. Fail. Anal.* 44 (2014) 250–271.
- [46] ASTM 1921-23, Test method for the determination of reference temperature  $T_0$  for ferritic steels in the transition range, ASTM International, West Conshohocken, USA, 2023.
- [47] S. Cicero, T. García, V. Madrazo, Application and validation of the notch master curve in medium and high strength structural steels, *J. Mech. Sci. Technol.* 29 (2015) 4129–4142.

- [48] V. Madrazo, S. Cicero, I.A. Carrascal, On the point method and the line method notch effect predictions in Al7075-T651, *Eng. Fract. Mech.* 79 (2012) 363–379.
- [49] S. Cicero, M. Sánchez, B. Arroyo, J.D. Fuentes, J.A. Álvarez, Estimation of the load-bearing capacity of tubular cantilever beams containing through-thickness circumferential U-notches, *Eng. Struct.* 229 (2021) 111598.
- [50] F.T. Ibáñez-Gutiérrez, S. Cicero, I.A. Carrascal, I. Procopio, Effect of fibre content and notch radius in the fracture behaviour of short glass fibre reinforced polyamide 6: An approach from the Theory of Critical Distances, *Compos. B Eng.* 94 (2016) 299–311.
- [51] F.T. Ibáñez-Gutiérrez, S. Cicero, Fracture assessment of notched short glass fibre reinforced polyamide 6: An approach from failure assessment diagrams and the theory of critical distances, *Compos B Eng.* 111 (2017) 124–133.
- [52] M. Sanchez, S. Arrieta, S. Cicero, V. Martínez-Mata, Fracture load predictions in additively manufactured ABS U-notched specimens using average strain energy density criteria, *Materials* 15 (2022) 2372.
- [53] S. Cicero, M. Sánchez, V. Martínez-Mata, S. Arrieta, B. Arroyo, Structural integrity assessment of additively manufactured ABS, PLA and graphene reinforced PLA notched specimens combining Failure Assessment Diagrams and the Theory of Critical Distances, *Theor. Appl. Fract. Mech.* 121 (2022) 103535.
- [54] ASTM D6068-10, Standard test methods for determining J-R curves of plastic materials, ASTM International, West Conshohocken, USA, 2010.
- [55] S. Cicero, V. Martínez-Mata, L. Castanon-Jano, A. Alonso-Estebanez, B. Arroyo, Analysis of notch effect in the fracture behaviour of additively manufactured PLA and graphene reinforced PLA, *Theor. Appl. Fract. Mech.* 114 (2021) 103032.
- [56] S. Cicero, S. Arrieta, M. Sánchez, L. Castanon-Jano, Analysis of additively manufactured notched PLA plates using failure assessment diagrams, *Theor. Appl. Fract. Mech.* 125 (2023) 103926.
- [57] F.T. Ibáñez-Gutiérrez, S. Cicero, I.A. Carrascal, On the influence of moisture content on the fracture behaviour of notched short glass fibre reinforced polyamide 6, *Compos. B Eng.* 159 (2019) 62–71.
- [58] S. Cicero, M. Sánchez, S. Arrieta, Predicting critical loads in fused deposition modeling graphene-reinforced PLA plates containing notches using the Point Method, *Polymers* 15 (18) (2023) 3797.
- [59] S. Cicero, T. García, J. Castro, V. Madrazo, D. Andrés, Analysis of notch effect on the fracture behaviour of granite and limestone: An approach from the Theory of Critical Distances, *Eng. Geol.* 177 (2014) 1–9.
- [60] J. Srawley, B. Gross, Cracks and fracture, *ASTM Spec Tech Publ.* 601 (1976) 559–579.
- [61] M. Kocak, S. Webster, J.J. Janosch, R.A. Ainsworth, R. Koers (Eds.), *FITNET Fitness-for-Service (FFS) Procedure*, vol. 1, GKSS, Germany, 2008.